Photoacoustics 25 (2022) 100321

Contents lists available at ScienceDirect

Photoacoustics

journal homepage: www.elsevier.com/locate/pacs

# Ppb-level gas detection using on-beam quartz-enhanced photoacoustic spectroscopy based on a 28 kHz tuning fork

Haoyang Lin [a], Huadan Zheng [a,*], Baiyang Antonio Zhou Montano [a], Hongpeng Wu [b], Marilena Giglio [c], Angelo Sampaolo [c], Pietro Patimisco [c], Wenguo Zhu [a], Yongchun Zhong [a], Lei Dong [b], Ruifeng Kan [d], Jianhui Yu [a], Vincenzo Spagnolo [c]

[a] Guangdong Provincial Key Laboratory of Optical Fiber Sensing and Communications, and Department of Optoelectronic Engineering, Jinan University, Guangzhou 510632, China
[b] State Key Laboratory of Quantum Optics and Quantum Optics Devices, Institute of Laser Spectroscopy, Shanxi University, Taiyuan 030006, China
[c] PolySense Lab, Dipartimento Interateneo di Fisica, University and Politecnico of Bari, CNR-IFN, Via Amendola 173, Bari 70126, Italy
[d] Key Laboratory of Environmental Optics and Technology, Anhui Institute of Optics and Fine Mechanics, Chinese Academy of Sciences, Hefei, China

ARTICLE INFO

*Keywords:*
Optical sensing
Photoacoustic spectroscopy
Quartz tuning fork
Quartz enhanced photoacoustic spectroscopy

ABSTRACT

In this paper, an on-beam quartz-enhanced photoacoustic spectroscopy (QEPAS) sensor based on a custom quartz tuning fork (QTF) acting as a photoacoustic transducer, was realized and tested. The QTF is characterized by a resonance frequency of 28 kHz, ~15% lower than that of a commercially available 32.7 kHz standard QTF. One-dimensional acoustic micro resonator (AmR) was designed and optimized by using stainless-steel capillaries. The 28 kHz QTF and AmRs are assembled in on-beam QEPAS configuration. The AmR geometrical parameters have been optimized in terms of length and internal diameter. The laser beam focus position and the AmR coupling distance were also adjusted to maximize the coupling efficiency. For comparison, QEPAS on-beam configurations based on a standard QTF and on the 28 kHz QTF were compared in terms of $H_2O$ and $CO_2$ detection sensitivity. In order to better characterize the performance of the system, $H_2O$, $C_2H_2$ and $CO_2$ were detected for a long time and the long-term stability was analyzed by an Allan variance analysis. With the integration time of 1 s, the detection limits for $H_2O$, $C_2H_2$ and $CO_2$ are 1.2 ppm, 28.8 ppb and 2.4 ppm, respectively. The detection limits for $H_2O$, $C_2H_2$ and $CO_2$ can be further improved to 325 ppb, 10.3 ppb and 318 ppb by increasing the integration time to 521 s, 183 s and 116 s

## 1. Introduction

Quartz-enhance photoacoustic spectroscopy (QEPAS), as a variant of photoacoustic spectroscopy (PAS), has been boomingly developed for trace gas detection during the past two decades [1]. The principle of PAS is that light sources were modulated to excite the molecules from ground state to excited states periodically. The deexcitation of molecules by vibration-translation (V-T) relaxation generates a periodical heating which further translates to acoustic waves [2]. A microphone was typically used as a transducer to convert acoustic waves to electrical signals. In QEPAS, a quartz tuning fork is employed as a highly sensitive optoacoustic transducer to detect the sound waves generated by the modulated excitation of the gas sample [3]. Indeed, as a piezoelectric acoustic transducer, QTF can convert the acoustic waves into electrical signals by the piezoelectric effect [4]. The employing of QTF results in normalized noise equivalent absorption coefficient up to ~$10^{-11}$ W $cm^{-1}$ $Hz^{-1/2}$, offering in addition immunity to ambient acoustic noise and capability to operate with acoustic detection modules having volume of a few $mm^3$ [5–7].

The QEPAS signal is given by the following equation:

$$S \propto \frac{Q \cdot P \cdot \alpha}{f_0} \tag{1}$$

where $S$, $P$ and $\alpha$ are the signal amplitude, laser power and absorption coefficient of molecules, respectively [8]. $Q$ and $f_0$ are the quality factor and resonance frequency of the QTF. Since 2002, most of the QEPAS sensing demonstrations have been performed using a standard QTF with a resonance frequency of 32768 Hz, the one used in clocks or watches for timing purposes. Operating at this high resonance frequency makes

* Corresponding author.
*E-mail addresses:* zhenghuadan@jnu.edu.cn (H. Zheng), donglei@sxu.edu.cn (L. Dong).

https://doi.org/10.1016/j.pacs.2021.100321
Received 3 November 2021; Received in revised form 3 December 2021; Accepted 5 December 2021
Available online 6 December 2021

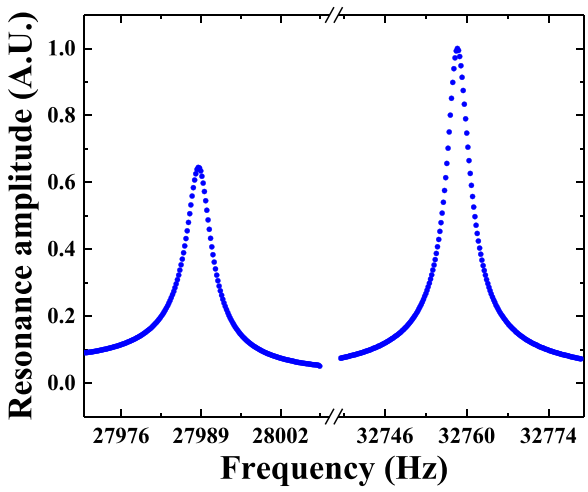


**Fig. 1.** Resonance curves measured for the 28 kHz QTF and a standard QTF.

**Table 1**
The electrical parameters of the 28 kHz QTF and standard QTF.

| Type | Resonance (Hz) | Q factor | Resistance (kΩ) |
|---|---|---|---|
| 28k QTF | 27,988.6 | 7730 | 202.5 |
| Standard QTF | 32,757.5 | 9726 | 130.7 |

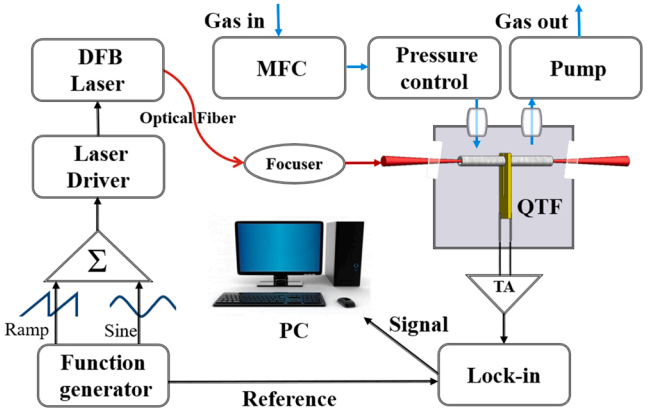


**Fig. 2.** QEPAS experimental setup based on 28 kHz QTF. DFB: distributed feedback; MFC: mass flow controller; QTF: quartz tuning fork; TA: transimpedance amplifier.

the QEPAS technique almost immune to $1/f$ noise and environmental acoustic noise. However, a stringent condition for PAS which has to be taken into account is that the molecular relaxation time $\tau$ should be much shorter than the modulation period, i.e., $\tau \ll 1/f$ [9], otherwise a signal amplitude reduction or phase shifts of the photoacoustic signal is expected. Indeed, when using a standard QTF for detection of molecules with a slow V-T relaxation, a signal amplitude reduction or phase shift always occurs [5].

To obtain higher QEPAS signals, custom QTFs with lower resonance frequencies were developed for QEPAS system since 2014 by Spagnolo et al. [10–14]. The availability of custom QTFs with a large prong spacing opened the way to the employment of high-power fiber-amplified near-IR lasers and THz lasers in QEPAS system [15–17,26], thanks to the reduction of the photothermal background noise caused by portion of the laser beam hitting the QTF, due to the poor beam quality of these laser sources. Several other breakthroughs in QEPAS development have been demonstrated using custom QTFs. Borri et al. used a distributed feedback quantum cascade laser for intracavity QEPAS sensor [18]. Patimisco et al. [19] and Sampaolo et al. [20] exploited custom tuning fork overtone modes for QEPAS detection. Wu et al. developed a sub-ppb level $H_2S$ sensor based on custom tuning fork with large prong spacing [21]. Zheng et al. developed the single tube on-beam QEPAS (SO-QEPAS) configuration to improve the detection SNR by $>100$ times for $CO_2$ detection [22]. Wang et al. developed a fiber-ring laser intracavity QEPAS gas sensor using a 7.2 kHz quartz tuning fork [23]. Giglio et al. designed two highly sensitive and easily interchangeable spectrophones based on custom quartz tuning forks [24]. Sun et al. realized ppb-Level CO detection in a $SF_6$ gas matrix exploiting a T-Grooved custom tuning fork [25]. Duquesnoy et al. demonstrated a normalized noise equivalent absorption (NNEA) of $3.7 \times 10^{-9}$ W cm$^{-1}$ Hz$^{-1/2}$ for $CO_2$ detection by using of custom tuning fork [26]. Most recently, Zheng et al. reported that pilot line manufactured custom quartz tuning forks with 28 kHz resonance frequency and $<10$ ppm frequency shift for gas detection [11].

In order to improve the QEPAS sensor performance, acoustic micro-resonators (AmR) are configured with a QTF to confine the sound waves and increase the signal amplitude [27]. AmR can be coupled with QTF in different configurations [28], being on-beam QEPAS [29] and off-beam QEPAS [30] the most commonly used configurations. The on-beam configuration produces strong signal-to-noise enhancement, the off-beam configuration avoids laser beam focusing through the QTF prongs, making easier the alignment and removing any background noise due to QTF illumination by the laser beam [31].

In this manuscript, an on-beam configuration was developed and optimized for a 28 kHz custom QTF. A pair of thin stainless-steel capillaries were assembled on each side of the QTF forming a one-dimensional acoustic resonator [32]. The length, inner diameter, and coupling position of the AmR were optimized in detail to improve the QEPAS sensor performance. The QEPAS sensor performance basing on standard 32.7 kHz QTF and 28 kHz QTF were compared by detecting molecules ($H_2O$ and $CO_2$) with different vibration-transition (V-T) relaxation times. Finally, the developed QEPAS sensor based on 28 kHz QTF was used for $H_2O$, $CO_2$ and $C_2H_2$ detection respectively. Allan variance was carried out to demonstrate the good long-term stability of the developed sensor.

## 2. Characterization of 28 kHz quartz tuning fork

Several 28 kHz QTFs were produced by custom pilot line as reported in our most recent publication [11]. The prongs length and thickness are 3.3 mm and 0.35 mm, respectively. The prongs spacing was set to 0.2 mm and the crystal thickness 0.4 mm. The electrical parameters of custom made 28 kHz QTF and standard 32.7 kHz QTF were compared. The electrical parameters were measured by using the system described in our previous publication ref [4] with a dedicated LabVIEW program. A sine signal with the bias voltage of 2 V and the peak-to-peak amplitude of 0.317 V was generated by a function generator (AFG3102, Tektronix) to drive the QTF. A lock-in amplifier (model SR830 DSP, SRS) was used for demodulation of the QTF output signal. The frequency of the sine signals was scanned from 27,970 Hz to 28,010 Hz and from 32,740 Hz to 32,780 Hz with a step of 0.2 Hz for 28 kHz QTF and standard QTF, respectively. Resonance curves of the 28 kHz QTF and standard QTF are shown in Fig. 1. The resonance frequency $f_0$, the quality factor $Q$ and the equivalent resistance $R$ obtained from the Lorentz fitting are listed in Table 1. The resonance frequency $f_0$ of 28 kHz QTF resulted 27,988.6 Hz, ~14.5% lower than that of the standard QTF. Referring to Eq. (1), this reduction of the resonance frequency should benefit the QEPAS signal. The full width at half maximum (FWHM) of two QTFs' resonance curve are similar (~3.3 Hz), as a result the 28 kHz QTF shows a ~ 20% lower Q factor with respect to the standard QTF.

## 3. Experimental setup

To evaluate the gas sensing performance of 28 kHz QTF, we

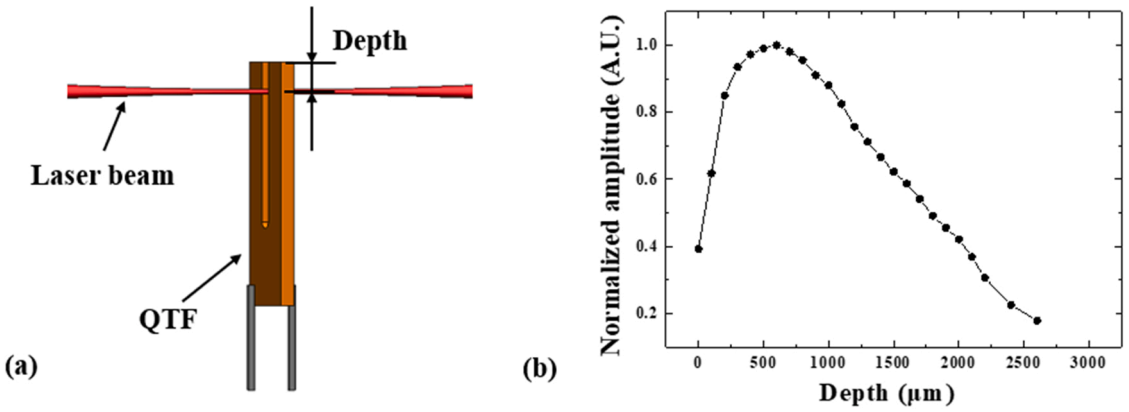


**Fig. 3.** (a) Position relationship between QTF and laser beam (b) Normalized QEPAS signal amplitude as the function of laser focus position depth.

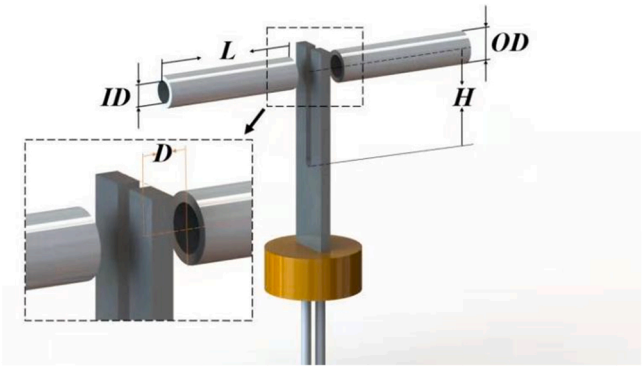


**Fig. 4.** The schematic diagram of on-beam QEPAS spectrophone.

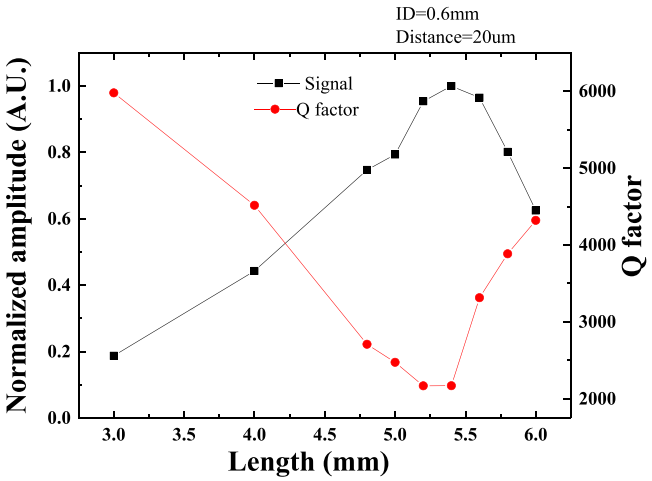


**Fig. 5.** QEPAS signal amplitude and QTF *Q* factor as the function of AmR length.

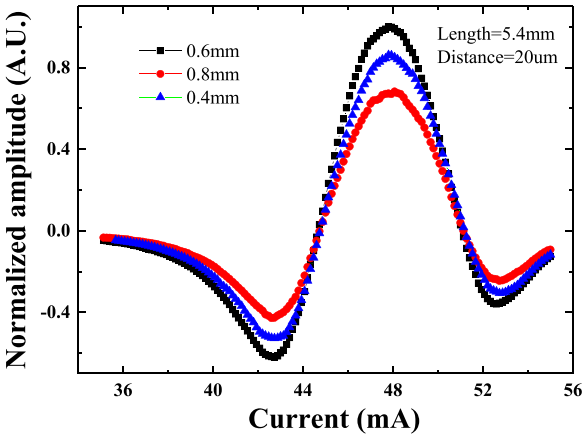


**Fig. 6.** Normalized QEPAS spectra obtained by using an AmR *ID* of 0.4 mm, 0.6 mm and 0.8 mm respectively.

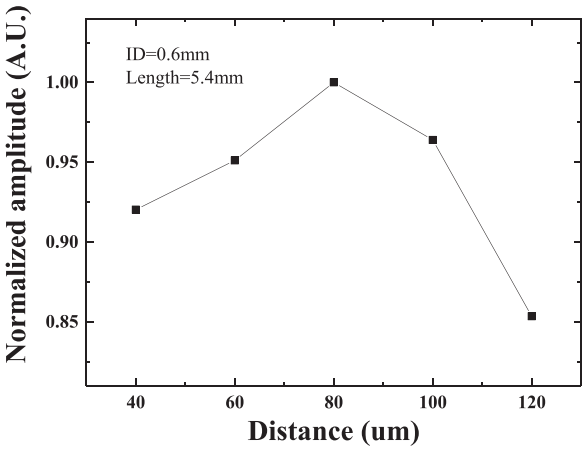


**Fig. 7.** Normalized signal amplitude as a function of the distance *D* between the microresonator tubes and the QTF.

employed the QEPAS experimental setup shown in Fig. 2. The second harmonic modulation method was exploited to improve the detection signal-to-noise ratio (SNR). The function generator (AFG3102) was used to generate a sine frequency with a frequency of $f_0/2$. A triangular signal with the frequency of 0.02 Hz and the sine signal were fed to the laser driver (Thorlabs CLD1015). The laser emission wavelength can be changed by controlling the injection current and the heat sink temperature. The modulated laser beam was focused by a fiber concentrator (OZ Optics). The focal length was 1 cm with a beam waist of ~0.1 mm. The laser beam passed through a window and focuses between the prongs of QTF. The acoustic waves generated by the photoacoustic effect were collected by QTF and then converted into electrical signals [29]. The electrical signals passed to a custom made transimpedance preamplifier with a feedback resistance of 10 MΩ, and the output signal was finally demodulated by a lock-in amplifier (SR830). The filter slope and time constant of the lock-in amplifier were set to 12 dB/Oct and 1 s, respectively. The system control and data process were carried out by a dedicated LabView program. All experiments in this work were carried

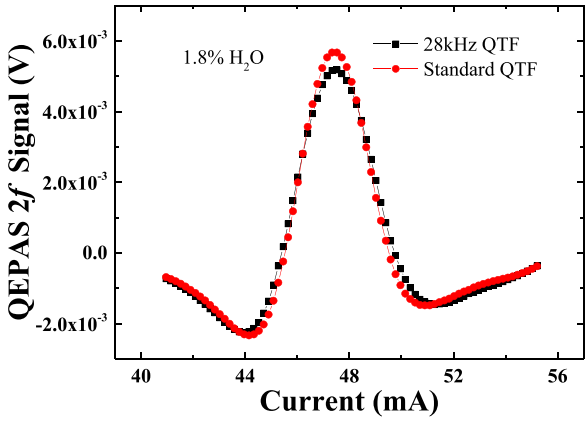


**Fig. 8.** QEPAS 2*f* signal measured using the 28 kHz QTF and standard QTF for $H_2O$ detection.

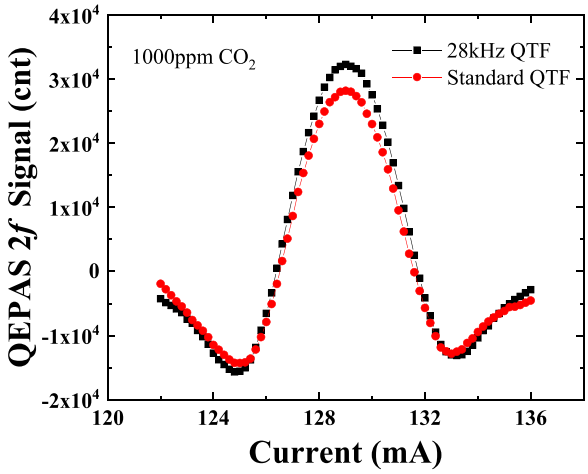


**Fig. 9.** Comparison of QEPAS 2*f* signal based on 28 kHz QTF and standard QTF when detecting $CO_2$.

out at room temperature and atmospheric pressure. The gas flow rate in the system was set to 100 standard cubic centimeters per minute (SCCM) by mass flow controller to avoid gas flow noise contributions.

## 4. Laser focus position effect of the 28 kHz QTF

The laser focus position with respect to QTF has significant impact on signal amplitude, Q-factor and signal-to-noise ratio (SNR) in QEPAS sensing [33,34]. Since 28 kHz QTF has a custom geometric size, the optimal focus position needs to be identified to improve the sensor performance. A DFB laser with a center wavelength of 1392 nm was used to measure the water vapor QEPAS signal and optimize the laser focus position. The laser temperature and injection current are set to 17.5 °C and 50 mA respectively to target the $H_2O$ absorption line at 7194.8 $cm^{-1}$ with an absorption intensity of 3.07 × $10^{-21}$ cm/mol. The water concentration was controlled at 1.8% by using Nafion humidifier (PermaPure). The laser focus position was moved along the QTF symmetry axe, from the QTF prong top to its base. The relationship between the normalized QEPAS signal amplitude and the laser focus position can be seen in Fig. 3. The depth represented the distance of the laser focal point from the QTF prong top, as shown in Fig. 3(a). As the depth gradually increased from 0, the amplitude of the signal gradually increased, then the QEPAS signal amplitude reached a maximum for a depth of ~600 μm. Since the laser beam must go through the AmR in on-beam QEPAS configuration, the depth of 600 μm was the height where we positioned the AmR.

## 5. Acoustic micro resonator design and optimization

The acoustic micro resonator (AmR) is a key component of the QEPAS spectrophone [27]. The schematic diagram of on-beam QEPAS spectrophone is shown in Fig. 4, where *L* is the length of each tube, *ID* is the tubes inner diameter, *OD* is the tubes outer diameter, *H* is the distance of the AmR symmetry axe from the prongs base and *D* is the AmR coupling distance. The coupling efficiency of AmRs and QTF strongly influences the Q factor and resonance frequency of the QEPAS spectrophone, as well as determines the signal amplitude and phase of the sensor.

According to the one-dimension acoustic resonator theory, the geometrical parameters of pipe resonator determines standing wave modes in the AmR [32]. In this section, the AmR length was optimized firstly. The AmR length should be an integer multiple of the half-wavelength of the sound wave. In this approximation, a nearly complete reflection of a dominant mode sound wave occurs at the open end of the resonator. However, in a resonator with an open end the antinode of a standing sound wave is located slightly outside the tubes end. The distance between the antinode and the tubes end is called open-end correction (OEC). The OEC is due to the effect of the air surrounding the resonator on the pressure field inside the tube [35]. As a result, the optimal on-beam AmR length, made up by two single stainless-steel capillary, should be $< \lambda/2$. The exact value has been determined experimentally. The AmR length was cut from 6 mm ($\lambda/2$) to 3 mm ($\lambda/4$) by numerical control machine tool. Each AmR was evaluate in terms of the signal amplitude and the QTF quality factor *Q*. The QEPAS signal amplitude and *Q* factor as the function of AmR length obtained are shown in Fig. 5. For a length of AmR of 5.4 mm, the quality factor Q decreased from 5978 to 2170, i.e., by more than 60%. A QTF is a high-*Q* resonator, however, is not used as a standalone sound wave detector, while it is acoustically coupled with an AmR. The acoustic coupling of the QTF with low-Q resonator tubes leads to a reduction of the overall spectrophone Q-factor due to an acoustic energy transfer between the QTF and AmR, but also to a strong enhance in QEPAS signal [29,36]. Under this condition, the QEPAS signal amplitude reached its maximum value, 5.33 times and 1.6 times larger than that measured for a length of 3 mm ($\lambda/4$) and 6 mm ($\lambda/2$), respectively.

With the AmR length of 5.4 mm, the distance *D* of ~ 20 μm and the QTF thickness of ~0.35 mm, the total length of the on-beam spectrophone is determined to be ~11.2 mm. In order to allow the laser beam to pass through the QEPAS spectrophone without touching the QTF and AmR, the inner diameter (*ID*) of AmR needs to be large enough. However, a too large resonator *ID* will reduce the sound enhancement effect. As a result, there is an optimum AmR *ID*. The influence of the AmR *ID* on the QEPAS signal amplitude can be seen in Fig. 6. For an optimized tube length of 5.4 mm and coupling distance *D* of 20 μm, the signal amplitude obtained by an AmR *ID* of 0.6 mm was 15% higher than the one measured for an *ID* = 0.4 mm and 45% higher than that obtained for *ID* = 0.8 mm.

The coupling distance *D* between the QTF plane and AmR has also an important influence on the QEPAS spectrophone performance. If AmR is too close to QTF, the amplitude of the signal will decrease due to the viscous damping. However, as the distance *D* increased, acoustic energy would leak from the gap and weaken the acoustic coupling of AmR with the QTF [37]. The optimized coupling effect can be achieved by finely tuning the distance *D*. The relationship between the normalized signal amplitude and the distance *D* can be observed in Fig. 7. The AmR length and *ID* were set at the optimized values of 5.4 mm and 0.6 mm, respectively. According to Fig. 7, when the coupling distance increased from 40 μm to 80 μm, the QEPAS signal amplitude also increases reaching a peak value. Indeed, at larger distances 80 μm the signal amplitude decreased. With an optimum coupling distance *D*= 80 μm, the obtained normalized amplitude was 8.7% higher than that measured

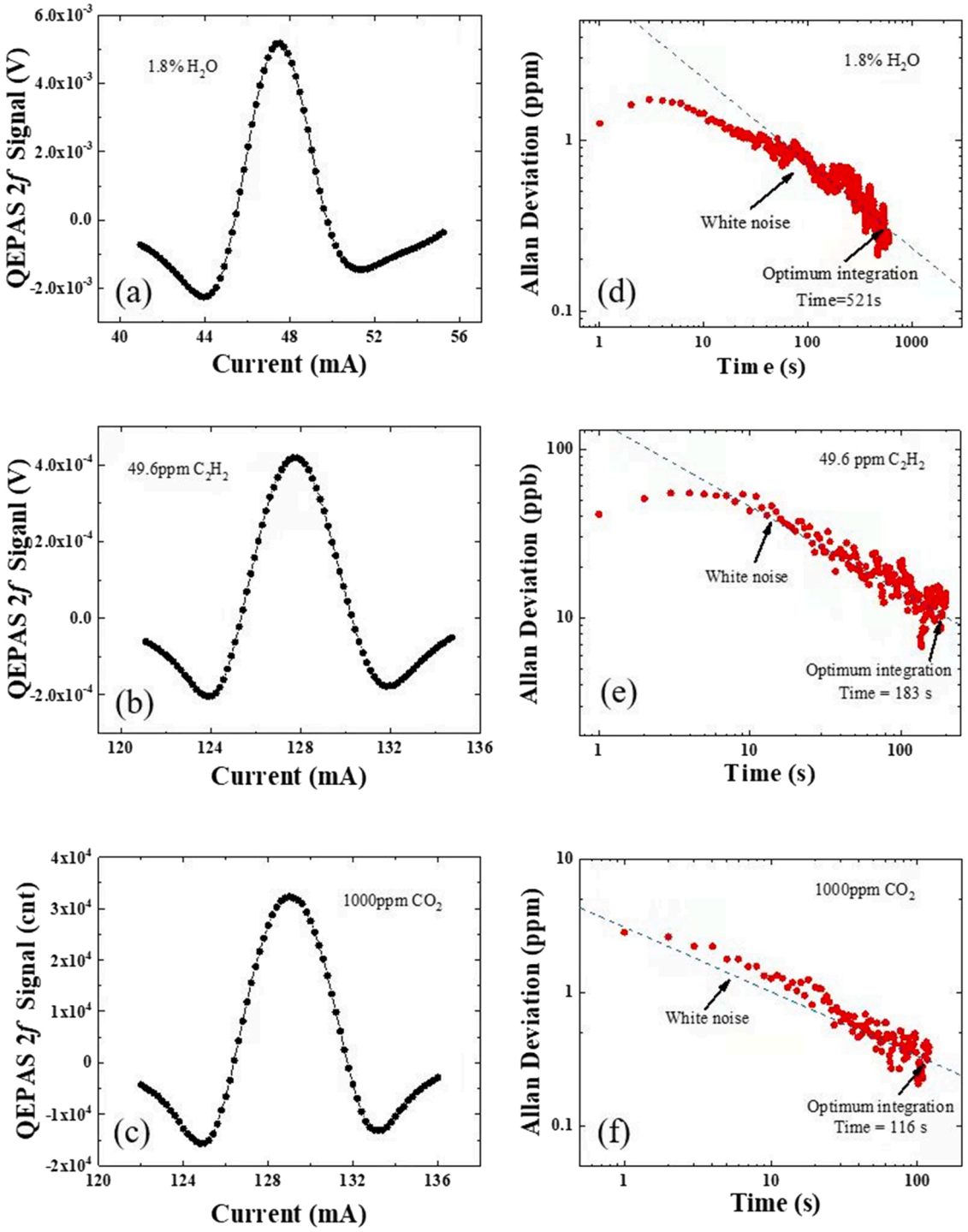


**Fig. 10.** QEPAS 2*f* signals and Allan deviations measured for $H_2O$, $C_2H_2$ and $CO_2$ with the 28 kHz QTF-based QEPAS systems.

for $D$= 40 μm. Thereby, the optimum AmR length, the ID and the coupling distance for an on-beam QEPAS configuration based on a 28 kHz QTF resulted 5.4 mm, 0.6 mm and 80 μm, respectively. With these optimal parameters, a signal enhancement factor of ~28 was achieved with respect to the bare 28 kHz QTF.

## 6. Comparison between 28 kHz QTF and standard QTF

When the modulation period is comparable with the molecular V-T relaxation time, a reduction on signal amplitude or phase shift is expected [38]. Under this condition, QTFs with a lower resonance frequency could improve the QEPAS performance. To compare the influence of the resonance frequency on QEPAS signal, QEPAS on-beam configurations based on 28 kHz QTF and standard QTF have been realized for the detection of $H_2O$ vapor and $CO_2$, i.e., a fast-and a slow-relaxing molecule, respectively.

Fig. 8 shows the 2*f* signals of the QEPAS spectrophones based on 28 kHz QTF and standard QTF when detecting $H_2O$. The injection current of a 1.39 μm DFB diode laser was tuned from 42 mA to 56 mA to scan a $H_2O$ absorption. A function generator (Tektronix) was used to modulate the laser while a lock-in amplifier (SRS) was used to retrieve the QEPAS 2*f* signal. The 28 kHz QTF was assembled in on-beam

**Table 2**
The detection limit and NNEA of the $CO_2$, $C_2H_2$ and $H_2O$ based on different QTF on-beam configuration QEPAS systems.

| | $H_2O$ | $C_2H_2$ | $CO_2$ |
|---|---|---|---|
| 15.2 kHz QTF | / | 94 ppb[40] $2.73 \times 10^{-9}$ cm$^{-1}$ W Hz$^{-1/2}$ | / |
| 32.7 kHz QTF | 1.058 ppm[41] | 2 ppm[42] $6.16 \times 10^{-8}$ cm$^{-1}$ W Hz$^{-1/2}$ | 18 ppm[43] $8.9 \times 10^{-9}$ cm$^{-1}$ W Hz$^{-1/2}$ |
| 30.7 kHz QTF | 4.3 ppm[44] | 33.2 ppb[a] [45] $3.54 \times 10^{-8}$ cm$^{-1}$ W Hz$^{-1/2}$ | / |
| 28 kHz QTF | 1.2 ppm [This paper]$3.1 \times 10^{-9}$ cm$^{-1}$ W Hz$^{-1/2}$ | 28.8 ppb [This paper] $1.1 \times 10^{-9}$ cm$^{-1}$ W Hz$^{-1/2}$ | 2.4 ppm [This paper]$8.3 \times 10^{-9}$ cm$^{-1}$ W Hz$^{-1/2}$ |

[a] power boosted by EDFA.

configuration with AmR length of 5.4 mm, *ID* of 0.6 and *D* of 80 μm, while the standard QTF was assembled in on-beam configuration with AmR length of 4.4 mm and *ID* of 0.6 mm, which resulted to be its optimal spectrophone configuration [29]. With 1.8% $H_2O$, the signal amplitude obtained with standard QTF was $5.67 \times 10^{-3}$ V, ~10% larger than that measured for the 28 kHz QTF. Being $H_2O$ a very fast relaxing molecule [2], the QEPAS signal is slightly influenced by the difference in resonance frequency between the two QTFs and the larger signal measured with the standard QTF can be attributed to its higher Q factor.

Fig. 9 shows the 2*f* QEPAS signals measured with the 28 kHz QTF and standard QTF when detecting $CO_2$. A field-programmable gate array (FPGA) control electronics unit (CEU) was used to drive and modulate a 2 μm diode laser and retrieve the 2*f* signal [39]. The unit of signal value was the analog-to-digital converter (ADC) counts (cnt). Each cnt in the signal obtained from the transimpedance preamplifier was equal to 1.8 nV rms. For $CO_2$, the obtained signal measured with the 28 kHz QTF QEPAS spectrophone resulted ~15% higher than that obtained with the standard QTF. The observed behavior is mostly due to difference in resonance frequency. Indeed, $CO_2$ molecules have quite slow V-T relaxation rate compared to the $H_2O$ molecules [5]. As a result, the QEPAS signal benefits from lower modulation frequency required by the 28 kHz QTF. Our results confirm that the 28 kHz QTF could show better performance when detecting molecules with low V-T relaxation rate such as $CO_2$, $NO_2$, CO etc.

## 7. Detection of $H_2O$, $C_2H_2$ and $CO_2$

To evaluate the performance of the 28 kHz QTF with on-beam configuration, $H_2O$, $C_2H_2$ and $CO_2$ molecules in $N_2$ were detected. A 1.39 μm DFB diode laser was used as the light source to cover the $H_2O$ absorption line falling at 7194.8 cm$^{-1}$ with a line intensity of $3.07 \times 10^{-21}$ cm/molecule. A 1.53 μm DFB diode laser was used to cover the $C_2H_2$ absorption line falling at 6534.3 cm$^{-1}$ with a line intensity of $1.21 \times 10^{-20}$ cm/molecule cm/molecule. A 2 μm DFB diode laser was used to cover the $CO_2$ absorption line falling at 4990.0 cm$^{-1}$ with a line intensity of $1.32 \times 10^{-21}$ cm/molecule.The concentration of $H_2O$ was controlled by a Nafion humidifier with a pure $N_2$ stream. Certified gas mixtures containing 49.6 ppm $C_2H_2$ in $N_2$ and 1000 ppm $CO_2$ in $N_2$ were provided by Dalian Date Gas Co. Ltd. The laser injection current was tuned from 40 mA to 55 mA, from 121 mA to 135 mA, and from 122 mA to 136 mA, to target the $H_2O$, $C_2H_2$ and $CO_2$ absorption line, respectively. Fig. 10 (a), (b), (c) shows the QEPAS 2*f* signals measured for $H_2O$, $C_2H_2$ and $CO_2$, The measured signal amplitude resulted $5.16 \times 10^{-3}$ V, $4.18 \times 10^{-4}$ V, and $3.23 \times 10^{4}$ cnt, respectively. The noise level was evaluated by tuning the laser wavelength away from the absorption lines. The obtained noise level for $H_2O$, $C_2H_2$ and $CO_2$ resulted $3.39 \times 10^{-7}$ V, $2.42 \times 10^{-7}$ V and $7.81 \times 10$ cnt, corresponding to a signal to noise ratio of about 15,220, 1720 and 414 respectively. SNR is obtained by dividing the 2 *f* signal peak value by 1σ noise. The detection limit was calculated by converting the noise level into a gas concentration. The detection sensitivities were also reported in Table 2. With an integration time of 1 s, the detection sensitivity for $H_2O$, $C_2H_2$ and $CO_2$ resulted 1.2 ppm, 28.8 ppb and 2.4 ppm respectively. A comparison of the detection limits and normalized noise equivalent absorption (NNEA) coefficients achieved by this work and other similar QEPAS sensors were reported in Table 2.

The minimum optical absorption coefficient detectable with a photoacoustic sensor is determined by a photoacoustic signal to noise (SNR) of 1. Usually, the noise is proportional to the detection bandwidth and the photoacoustic signal is proportional to optical power, respectively. As a result, the laser-independent value characterizing a photoacoustic sensor is the NNEA, determined as the minimum optical absorption coefficient multiplied by the optical excitation power and divided by the detector bandwidth. NNEA can be expressed as [26]:

$$NNEA = \frac{P \times a}{SNR \times \sqrt{\Delta f}}$$

where *P* is the average optical power, *α* is the gas absorption coefficient, Δ*f* is the detection bandwidth, and *SNR* is the detection signal to noise ratio, respectively. Considering a detection bandwidth of 0.25 Hz, the calculated NNEA of the developed sensor for $H_2O$, $C_2H_2$ and $CO_2$ , result $3.1 \times 10^{-9}$ cm$^{-1}$ W Hz$^{-1/2}$, $1.1 \times 10^{-9}$ cm$^{-1}$ W Hz$^{-1/2}$ and $8.3 \times 10^{-9}$ cm$^{-1}$ W Hz$^{-1/2}$, respectively.

Allan deviation was performed to evaluate the long-term stability of the developed sensor. The standard deviation decreased as the integration time increased, indicating that the John White noise dominates in the QEPAS system. The optimum integration time for $H_2O$, $C_2H_2$ and $CO_2$ detection resulted ~521 s, ~183 s and ~116 s respectively. With these optimal integration times, detection limits of ~325 ppb, ~10.3 ppb and ~318 ppb were achieved for $H_2O$, $C_2H_2$ and $CO_2$ respectively.

## 8. Conclusions

In this paper, an on-beam quartz-enhanced photoacoustic spectroscopy sensor based on a 28 kHz QTF was demonstrated. An optimal one-dimensional longitudinal AmR was realized to improve the resonance enhancement of acoustic waves. With an AmR length of 5.4 mm, *ID* of 0.6 mm, and coupling distance *D* of 80 μm the optimized on-beam QEPAS configuration achieved a signal enhancement factor of ~28, compared to the bare QTF. The 28 kHz QTF was compared with a standard 32 kHz QTF for the detection of fast ($H_2O$) and slow ($CO_2$) relaxing molecules. When detecting $H_2O$ the standard QTF provides an higher signal due to its larger Q factor. However, when targeting $CO_2$ characterized by a large V-T relaxation time, the QEPAS signal obtained with the 28 kHz QTF was 15% higher than that of the standard QTF. In order to further test the performance of the 28 kHz QTF-based QEPAS sensor, $H_2O$, $C_2H_2$, and $CO_2$ in an $N_2$ matrix were detected. With an integration time of 1 s, detection limits of 1.2 ppm, 28.8 ppb and 2.4 ppm were achieved for $H_2O$, $C_2H_2$, and $CO_2$ detection, respectively. The long-term stability of the 28 kHz QTF-based QEPAS sensor was investigated by an Allan deviation analysis. With integration time of ~521 s, ~183 s and ~116 s, the detection limit for $H_2O$, $C_2H_2$, and $CO_2$ can be further improved up to ~325 ppb, ~10.3 ppb and ~318 ppb, respectively. A comparison of the achieved results with data reported in literature confirms the performances of the developed sensor system. Compared to a standard 32 kHz QTF, the detectivity level for $H_2O$ is comparable, however the 28 kHz QTF shows a better performance for $CO_2$ detection. The reason can be attributed to that the different V-T relaxation time of $H_2O$ and $CO_2$. $H_2O$ is a fast-relaxing molecule, also used as relaxation promoter for QEPAS, thereby a reduction of resonance frequency does not affect its QEPAS response, while $CO_2$ is a slow relaxer and thereby a reduction of resonance frequency is helpful in terms of energy transfer to $N_2$. For example, around 2 μm wavelength range $H_2O$-$N_2$ and $CO_2$-$N_2$ show relaxation times of ~11 μs and ~110 μs

respectively [5].

Further improvement can be made on the optimization of the AmR length and corresponding coupling distance, since variation in coupling distance may influence the optimal AmR length. The developed configuration can also show advantages in the photothermal spectroscopy [46] or light-induced thermoelastic spectroscopy [47].

## Declaration of Competing Interest

The authors declare that they have no known competing financial interests or personal relationships that could have appeared to influence the work reported in this paper.

## Acknowledgment

This work is supported by the National Natural Science Foundation of China (12174156, 12174155, 62005105, 62075088), Natural Science Foundation of Guangdong Province (2020B1515020024, 2017A030313375, 2019A1515011380), National Key Research and Development Program of China (2021YFB2800801), Key-Area Research and Development Program of Guangdong Province (2019B010138004, 2017A010102006), Project of Guangzhou Industry Leading Talents (CXLJTD-201607), and Planned Science & Technology Project of Guangzhou (201707010396), Aeronautical Science Foundation of China (201808W4001), Special Project in Key Fields of the Higher Education Institutions of Guangdong Province (2020ZDZX3022), Open foundation of CEPREI (NO. 19D09), Foundation for Distinguished Young Talents in Higher Education of Guangdong (2018KQNCX009), the Fundamental Research Funds for the Central Universities (21619402, 11618413), State Key Laboratory of Applied Optics (SKLAO-201914).

## References

[1] A.A. Kosterev, Y.A. Bakhirkin, R.F. Curl, F.K. Tittel, Quartz-enhanced photoacoustic spectroscopy, Opt. Lett. 27 (2002) 1902–1904.
[2] S. Dello Russo, A. Sampaolo, P. Patimisco, G. Menduni, M. Giglio, C. Hoelzl, V.M. N. Passaro, H. Wu, L. Dong, V. Spagnolo, Quartz-enhanced photoacoustic spectroscopy exploiting low-frequency tuning forks as a tool to measure the vibrational relaxation rate in gas species, Photoacoustics 21 (2021), 100227.
[3] Y. Ma, R. Lewicki, M. Razeghi, F.K. Tittel, QEPAS based ppb-level detection of CO and $N_2O$ using a high power CW DFB-QCL, Opt. Express 21 (2013) 1008–1019.
[4] H. Wu, L. Dong, H. Zheng, Y. Yu, W. Ma, L. Zhang, W. Yin, L. Xiao, S. Jia, F. K. Tittel, Beat frequency quartz-enhanced photoacoustic spectroscopy for fast and calibration-free continuous trace-gas monitoring, Nat. Commun. 8 (2017) 1–8.
[5] G. Wysocki, A.A. Kosterev, F.K. Tittel, Influence of molecular relaxation dynamics on quartz-enhanced photoacoustic detection of $CO_2$ at $\lambda = 2$ μm, Appl. Phys. B 85 (2) (2006) 301–306.
[6] P. Patimisco, A. Sampaolo, L. Dong, F.K. Tittel, V. Spagnolo, Recent advances in quartz enhanced photoacoustic sensing, Appl. Phys. Rev. 5 (2018), 011106.
[7] Y. Liu, H. Zheng, H. Lin, B.A. Zhou Montano, W. Zhu, Y. Zhong, R. Kan, B. Yuan, J. Yu, M. Shao, Integrated mid-infrared QEPAS sensor basing on a 28 kHz quartz tuning fork for online monitoring of CO2 in the greenhouse, Photoacoustics (2021).
[8] Y. Ma, Y. He, X. Yu, C. Chen, R. Sun, F.K. Tittel, HCl ppb-level detection based on QEPAS sensor using a low resonance frequency quartz tuning fork, Sens. Actuators B-Chem. 233 (2016) 388–393.
[9] P. Breitegger, B. Schweighofer, H. Wegleiter, M. Knoll, B. Lang, A. Bergmann, Towards low-cost QEPAS sensors for nitrogen dioxide detection, Photoacoustics 18 (2020), 100169.
[10] A. Sampaolo, P. Patimisco, M. Giglio, A. Zifarelli, H. Wu, L. Dong, V. Spagnolo, Quartz-enhanced photoacoustic spectroscopy for multi-gas detection: a review, Anal. Chim. Acta 1188 (2021), 338894.
[11] H. Zheng, Y. Liu, H. Lin, B. Liu, X. Gu, D. Li, B. Huang, Y. Wu, L. Dong, W. Zhu, J. Tang, H. Guan, H. Lu, Y. Zhong, J. Fang, Y. Luo, J. Zhang, J. Yu, Z. Chen, F. K. Tittel, Quartz-enhanced photoacoustic spectroscopy employing pilot line manufactured custom tuning forks, Photoacoustics 17 (2020), 100158.
[12] R. Cui, H. Wu, L. Dong, W. Chen, F.K. Tittel, Multiple-sound-source-excitation quartz-enhanced photoacoustic spectroscopy based on a single-line spot pattern multi-pass cell, Appl. Phys. Lett. 118 (2021), 161101.
[13] S. Dello Russo, S. Zhou, A. Zifarelli, P. Patimisco, A. Sampaolo, M. Giglio, D. Iannuzzi, V. Spagnolo, Photoacoustic spectroscopy for gas sensing: a comparison between piezoelectric and interferometric readout in custom quartz tuning forks, Photoacoustics 17 (2020), 100155.
[14] M. Lassen, L. Lamard, Y. Feng, A. Peremans, J.C. Petersen, Off-axis quartz-enhanced photoacoustic spectroscopy using a pulsed nanosecond mid-infrared optical parametric oscillator, Opt. Lett. 41 (2016) 4118–4121.
[15] H. Wu, L. Dong, H. Zheng, X. Liu, X. Yin, W. Ma, L. Zhang, W. Yin, S. Jia, F.K. Tittel, Enhanced near-infrared QEPAS sensor for sub-ppm level $H_2S$ detection by means of a fiber amplified 1582 nm DFB laser, Sens. Actuators B-Chem. 221 (2015) 666–672.
[16] S. Borri, P. Patimisco, A. Sampaolo, H.E. Beere, D.A. Ritchie, M.S. Vitiello, G. Scamarcio, V. Spagnolo, Terahertz quartz enhanced photo-acoustic sensor, Appl. Phys. Lett. 103 (2013), 021105.
[17] A. Sampaolo, C. Yu, T. Wei, A. Zifarelli, M. Giglio, P. Patimisco, H. Zhu, H. Zhu, L. He, H. Wu, L. Dong, G. Xu, V. Spagnolo, $H_2S$ quartz-enhanced photoacoustic spectroscopy sensor employing a liquid-nitrogen-cooled THz quantum cascade laser operating in pulsed mode, Photoacoustics 21 (2021), 100219.
[18] S. Borri, P. Patimisco, I. Galli, D. Mazzotti, G. Giusfredi, N. Akikusa, M. Yamanishi, G. Scamarcio, P.D. Natale, V. Spagnolo, Intracavity quartz-enhanced photoacoustic sensor, Appl. Phys. Lett. 104 (9) (2014), 091114.
[19] P. Patimisco, A. Sampaolo, M. Giglio, V. Mackoviak, H. Rossmadl, B. Gross, A. Cable, F.K. Tittel, V. Spagnolo, Octupole electrode pattern for tuning forks vibrating at the first overtone mode in quartz-enhanced photoacoustic spectroscopy, Opt. Lett. 43 (2018) 1854–1857.
[20] A. Sampaolo, P. Patimisco, L. Dong, A. Geras, G. Scamarcio, T. Starecki, F.K. Tittel, V. Spagnolo, Quartz-enhanced photoacoustic spectroscopy exploiting tuning fork overtone modes, Appl. Phys. Lett. 107 (23) (2015), 231102.
[21] H. Wu, A. Sampaolo, L. Dong, P. Patimisco, X. Liu, H. Zheng, X. Yin, W. Ma, L. Zhang, W. Yin, V. Spagnolo, S. Jia, F.K. Tittel, Quartz enhanced photoacoustic $H_2S$ gas sensor based on a fiber-amplifier source and a custom tuning fork with large prong spacing, Appl. Phys. Lett. 107 (11) (2015), 111104.
[22] H. Zheng, L. Dong, A. Sampaolo, H. Wu, P. Patimisco, X. Yin, W. Ma, L. Zhang, W. Yin, V. Spagnolo, S. Jia, F.K. Tittel, Single-tube on-beam quartz-enhanced photoacoustic spectroscopy, Opt. Lett. 41 (5) (2016) 978–981.
[23] Q. Wang, Z. Wang, W. Ren, P. Patimisco, A. Sampaolo, V. Spagnolo, Fiber-ring laser intracavity QEPAS gas sensor using a 7.2 kHz quartz tuning fork, Sens. Actuators B-Chem. 268 (2018) 512–518.
[24] M. Giglio, A. Elefante, P. Patimisco, A. Sampaolo, F. Sgobba, H. Rossmadl, V. Mackowiak, H. Wu, F.K. Tittel, L. Dong, V. Spagnolo, Quartz-enhanced photoacoustic sensor for ethylene detection implementing optimized custom tuning fork-based spectrophone, Opt. Express 27 (4) (2019) 4271–4280.
[25] B. Sun, A. Zifarelli, H. Wu, S. Dello Russo, S. Li, P. Patimisco, L. Dong, V. Spagnolo, Mid-infrared quartz-enhanced photoacoustic sensor for ppb-Level CO detection in a $SF_6$ gas matrix exploiting a T-grooved quartz tuning fork, Anal. Chem. 92 (20) (2020) 13922–13929.
[26] M. Duquesnoy, G. Aoust, J.-M. Melkonian, R. Lévy, M. Raybau, A. Godard, Quartz enhanced photoacoustic spectroscopy based on a custom quartz tuning fork, Sensors 19 (6) (2019) 1362.
[27] H. Zheng, L. Dong, P. Patimisco, H. Wu, A. Sampaolo, X. Yin, S. Li, W. Ma, L. Zhang, W. Yin, L. Xiao, V. Spagnolo, S. Jia, F.K. Tittel, Application of acoustic micro-resonators in quartz-enhanced photoacoustic spectroscopy for trace gas analysis, Chem. Phys. Lett. 691 (2018) 462–472.
[28] L. Hu, C. Zheng, M. Zhang, D. Yao, J. Zheng, Y. Zhang, Y. Wang, F.K. Tittel, Quartz-enhanced photoacoustic spectroscopic methane sensor system using a quartz tuning fork-embedded, double-pass and off-beam configuration, Photoacoustics 18 (2020), 100174.
[29] L. Dong, A.A. Kosterev, D. Thomazy, F.K. Tittel, QEPAS spectrophones: design, optimization, and performance, Appl. Phys. B 100 (2010) 627–635.
[30] K. Liu, X. Guo, H. Yi, W. Chen, W. Zhang, X. Gao, Off-beam quartz-enhanced photoacoustic spectroscopy, Opt. Lett. 34 (2009) 1594–1596.
[31] P. Patimisco, G. Scamarcio, F.K. Tittel, V. Spagnolo, Quartz-enhanced photoacoustic spectroscopy: a review, Sensors 14 (4) (2014) 6165–6206.
[32] A. Miklós, P. Hess, Z. Bozóki, Application of acoustic resonators in photoacoustic trace gas analysis and metrology, Rev. Sci. Instrum. 72 (4) (2001) 1937–1955.
[33] H. Lin, Z. Huang, R. Kan, H. Zheng, Y. Liu, B. Liu, L. Dong, W. Zhu, J. Tang, J. Yu, Z. Chen, F.K. Tittel, Application of micro quartz tuning fork in trace gas sensing by use of quartz-enhanced photoacoustic spectroscopy, Sensors 19 (23) (2019) 5240.
[34] H. Wu, L. Dong, W. Ren, W. Yin, W. Ma, L. Zhang, S. Jia, F.K. Tittel, Position effects of acoustic micro-resonator in quartz enhanced photoacoustic spectroscopy, Sens. Actuators B Chem. 206 (2015) 364–370.
[35] S. Dello Russo, M. Giglio, A. Sampaolo, P. Patimisco, G. Menduni, H. Wu, L. Dong, Vittorio M.N. Passaro, V. Spagnolo, Acoustic coupling between resonator tubes in quartz-enhanced photoacoustic spectrophones employing a large prong spacing tuning fork, Sensors 19 (19) (2019) 4109.
[36] S. Dello Russo, M. Giglio, A. Sampaolo, P. Patimisco, G. Menduni, H. Wu, L. Dong, V.M.N. Passaro, V. Spagnolo, Acoustic coupling between resonator tubes in quartz-enhanced photoacoustic spectrophones employing a large prong spacing Tuning fork, sensors 19 (2019) 4109.
[37] Y. Cao, W. Jin, H.L. Ho, Optimization of spectrophone performance for quartz-enhanced photoacoustic spectroscopy, Sens. Actuators B-Chem. 174 (2012) 24–30.
[38] A.A. Kosterev, Y.A. Bakhirkin, F.K. Tittel, Ultrasensitive gas detection by quartz-enhanced photoacoustic spectroscopy in the fundamental molecular absorption bands region, Appl. Phys. B 80 (1) (2005) 133–138.
[39] S. Schilt, A.A. Kosterev, F.K. Tittel, Performance evaluation of a near infrared QEPAS based ethylene sensor, Appl. Phys. B 95 (4) (2009) 813–824.
[40] S. Li, H. Wu, R. Cui, A. Sampaolo, P. Patimisco, V. Spagnolo, F.K. Tittel, L. Dong, Piezo-enhanced acoustic detection module for mid-infrared trace gas sensing using a grooved quartz tuning fork, Opt. Express 27 (24) (2019) 35267–35278.
[41] P. Gong, X. Liang, X. Qi, R. Wang, H. Wang, M. Chang, H. Yang, F. Sun, G. Li, A quartz-enhanced photoacoustic spectroscopy sensor for measurement of water vapor concentration in the air, Chin. Phys. B 24 (1) (2015), 014206.

[42] Y. Cao, W. Jin, H.L. Ho, L. Qi, Y.H. Yang, Acetylene detection based on diode laser QEPAS: combined wavelength and residual amplitude modulation, Appl. Phys. B 109 (2) (2012) 359–366.
[43] R. Lewicki, G. Wysocki, A.A. Kosterev, F.K. Tittel, Carbon dioxide and ammonia detection using 2 μm diode laser based quartz-enhanced photoacoustic spectroscopy, Appl. Phys. B 87 (1) (2007) 157–162.
[44] Y. Ma, G. Yu, J. Zhang, X. Yu, R. Sun, F.K. Tittel, Quartz enhanced photoacoustic spectroscopy based trace gas sensors using different quartz tuning forks, Sensors 15 (4) (2015) 7596–7604.
[45] Y. Ma, Y. He, L. Zhang, X. Yu, J. Zhang, R. Sun, F.K. Tittel, Ultra-high sensitive acetylene detection using quartz-enhanced photoacoustic spectroscopy with a fiber amplified diode laser and a 30.72 kHz quartz tuning fork, Appl. Phys. Lett. 110 (2017), 031107.
[46] Y. Ma, Y. Hu, S. Qiao, Y. He, F.K. Tittel, Trace gas sensing based on multi-quartz-enhanced photothermal spectroscopy, Photoacoustics 20 (2020), 100206.
[47] S. Qiao, Y. Ma, Y. He, P. Patimisco, A. Sampaolo, V. Spagnolo, Ppt level carbon monoxide detection based on light-induced thermoelastic spectroscopy exploring custom quartz tuning forks and a mid-infrared QCL, Opt. Express 29 (2021) 25100–25108.

**Haoyang Lin** received his bachelor's degree on department of optoelectronic engineering from Jinan University, Guangzhou, China. He is now pursuing a master's degree in Department of Optoelectronic Engineering at Jinan University, China. His recent research His research interests include gas sensor, photoacoustic spectroscopy, and laser spectroscopy.

**Huadan Zheng** received his Ph.D. degree in atomic and molecular physics from Shanxi university, China, in 2018. From 2016–2017, he studied as a joint Ph.D. student in the electrical and computer engineering department and rice quantum institute, Rice University, Houston, USA. Currently he is an associate professor in the Department of Optoelectronic Engineering of Jinan University. His research interests include optical sensors and laser spectroscopy techniques.

**Baiyang Antonio Zhou Montano** is now pursuing a bachelor's degree in information engineering in the Department of Photoelectric Engineering of Jinan university. His research interests include optical fiber sensing, signal acquisition and processing, automation, control, and intelligent systems

**Hongpeng Wu** received his Ph.D. degree in atomic and molecular physics from Shanxi University, China, in 2017. From September 2015 to October 2016, he studied as a joint Ph.D. student in the Electrical and Computer Engineering Department and Rice Quantum Institute, Rice University, Houston, USA. Currently he is a full professor in the Institute of Laser Spectroscopy of Shanxi University. His research interests include gas sensors, photoacoustic spectroscopy, photothermal spectroscope and laser spectroscopy techniques.

**Marilena Giglio** received the M.S. degree in Applied Physics in 2014, and the PhD Degree in Physics in 2018 from the University of Bari. In 2012 she's been visiting the Academic Medical Center of Amsterdam as a trainee. In 2015 she was a Research Assistant with the Department of Physics, University of Bari. She was a visiting researcher in the Laser Science Group at Rice University from 2016 to 2017. Since 2018, she is a Post-Doc Research Assistant at the Physics Department of the Technical University of Bari. Her research activity is focused on the development of gas sensors based on Quartz-Enhanced Photoacoustic Spectroscopy and on the op-tical coupling of hollow-core waveguides with interband- and quantum-cascade lasers.

**Angelo Sampaolo** obtained his master's degree in physics in 2013 and the Ph.D Degree in Physics in 2017 from University of Bari. He was an associate researcher in the Laser Science Group at Rice University from 2014 to 2016 and associate researcher at Shanxi University since 2018. Since May 2017, he was a Post-Doctoral Research associate at University of Bari and starting from December 2019, he is Assistant Professor at Polytechnic of Bari. His research activity has included the study of the thermal properties of heterostructure devices via Raman spectroscopy. Most recently, his research interest has focused on the development of innovative techniques in trace gas sensing, based on Quartz-Enhanced Photoacoustic Spectros copy and covering the full spectral range from near-IR to THz. His achieved results have been acknowledged by a cover paper in Applied Physics Letter of the July 2013 issue.

**Pietro Patimisco** obtained the master's degree in physics in 2009 and the PhD Degree in Physics in 2013 from the University of Bari. Since 2018, he is Assistant professor at the Technical University of Bari. He was a visiting scientist in the Laser Science Group at Rice University in 2013 and 2014. Dr. Patimisco's scientific activity addressed both micro-probe optical characterization of semiconductor optoelectronic devices and optoacoustic gas sensors. Recently, his research activities included the study and applications of trace-gas sensors, such as quartz enhanced photoacoustic spectroscopy and cavity enhanced absorption spectroscopy in the mid infrared and terahertz spectral region, leading to several publications, including a cover paper in Applied Physics Letter of the July 2013 issue.

**Wenguo Zhu** is now an associate professor in Department of Optoelectronic Engineering at Jinan University, China. He got both his Ph. D. degree on Optics in 2016 and his bachelor's degree on optical information in 2011 from Sun Yet-Sen University, China. Currently he is an associate professor in the Department of Optoelectronic Engineering of Jinan University. His recent research interests include optical spin and orbital angular momentum, zero-index metamaterial, novel nanophotonic devices, and novel optical fiber sensors.

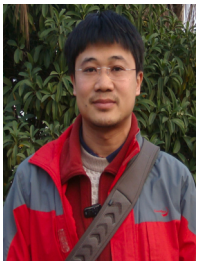

**Yongchun Zhong** received the Ph.D. degree in optics from Sun Yat-sen University, Guangzhou, China, in 2004. Then, he did postdoctoral research with the Hong Kong University of Science and Technology from 2004 to 2009. He is an full professor with the Jinan University, Guangzhou, China. He has authored more than 30 journal papers. His current research interests include photonic crystal fiber devices, holography, and photoelectric material.

**Jianhui Yu** is a professor in Department of Optoelectronic Engineering at Jinan University, China. He got both his Ph. D. degree on optical engineering in 2009 and his bachelor's degree on physics in 2002 from Sun Yet-Sen University, China. Currently he is a full professor in the Department of Optoelectronic Engineering of Jinan University. His recent research interests include novel micro/nano fiber-based optical devices, all optical controllable devices, optical momentum in dielectric media and in waveguide, measurement and application of optical force, and novel optical fiber sensors.

**Ruifeng Kan** received his Ph.D. degree from Anhui Institute of Optics and Fine Mechanics, CAS. His research interests focus on laser spectroscopy and its application in environmental pollution, production safety, aerospace flow field diagnosis, and deep sea dissolved gas detection.

**Lei Dong** received his Ph.D. degree in optics from Shanxi University, China, in 2007. From June, 2008 to December, 2011, he worked as a post-doctoral fellow in the Electrical and Computer Engineering Department and Rice Quantum Institute, Rice University, Houston, USA. Currently he is a professor in the Institute of Laser Spectroscopy of Shanxi University. His research interests include optical sensors, trace gas detection, photoacoustic spectroscopy and laser spectroscopy.

**Vincenzo Spagnolo** obtained the PhD in physics in 1994 from University of Bari. From 1997–1999, he was researcher of the National Institute of the Physics of Matter. Since 2004, he works at the Technical University of Bari, formerly as assistant and associate professor and now as full Professor of Physics. Starting from 2019, he become Vice-Rector of the technical university of Bari - Deputy to Technology Transfer. He is the director of the joint-research lab PolySense between Technical University of Bari and THORLABS GmbH, fellow member of SPIE and senior member of OSA. His research interests include optoacoustic gas sensing and spectroscopic techniques for real-time monitoring. His research activity is documented by more than 210 publications and 3 filed patents. He has given more than 50 invited presentations at international conferences and workshops.